Self-calibrating common-path interferometry

Rosario Porras-Aguilar,[1,2,*] Konstantinos Falaggis,[3] Julio C. Ramirez-San-Juan,[4] and Ruben Ramos-Garcia[4]

[1]*Consejo Nacional de Ciencia y Tecnologia, Av. Insurgentes Sur 1582, 03940, México, D.F,. Mexico*
[2]*Technologic Development Direction, Instituto Nacional de Astrofisica, Optica y Electronica, Luis Erro 1, 72840 Puebla, Mexico*
[3]*Institute of Micromechanics and Photonics, Warsaw University of Technology, 8 Sw A. Boboli Str, 02-525 Warsaw, Poland*
[4]*Optics Departament, Instituto Nacional de Astrofisica, Optica y Electronica, Luis Erro 1, 72840 Puebla, Mexico*
[*]rporras@inaoep.mx

Abstract: A quantitative phase measuring technique is presented that estimates the object phase from a series of phase shifted interferograms that are obtained in a common-path configuration with unknown phase shifts. The derived random phase shifting algorithm for common-path interferometers is based on the Generalized Phase Contrast theory [Appl. Opt. **40**(2), 268 (2001)], which accounts for the particular image formation and includes effects that are not present in two-beam interferometry. It is shown experimentally that this technique can be used within common-path configurations employing nonlinear liquid crystal materials as self-induced phase filters for quantitative phase imaging without the need of phase shift calibrations. The advantages of such liquid crystal elements compared to spatial light modulator based solutions are given by the cost-effectiveness, self-alignment, and the generation of diminutive dimensions of the phase filter size, giving unique performance advantages.

OCIS codes: (120.3180) Interferometry; (120.5050) Phase measurement; (160.3710) Liquid crystals; (180.3170) Interference microscopy; (230.3720) Liquid-crystal devices.

References and links

1. K. A. Nugent, D. Paganin, and T. E. Gureyev, "A Phase Odyssey," Phys. Today **54**(8), 27–32 (2001).
2. F. Zernike, "Phase contrast, a new method for the microscopic observation of transparent objects - Part I," Physica **9**(7), 686–698 (1942).
3. D. Malacara-Hernandez, *Optical Shop Testing* (John Wiley & Sons, Inc., 2007).
4. M. Servin, D. Malacara, and J. L. Marroquin, "Wave-front recovery from two orthogonal sheared interferograms," Appl. Opt. **35**(22), 4343–4348 (1996).
5. K. Creath, "Step height measurement using two-wavelength phase-shifting interferometry," Appl. Opt. **26**(14), 2810–2816 (1987).
6. J. C. Wyant, "Testing aspherics using two-wavelength holography," Appl. Opt. **10**(9), 2113–2118 (1971).
7. Z. Jingshan, R. A. Claus, J. Dauwels, L. Tian, and L. Waller, "Transport of Intensity phase imaging by intensity spectrum fitting of exponentially spaced defocus planes," Opt. Express **22**(9), 10661–10674 (2014).
8. K. Falaggis, T. Kozacki, and M. Kujawinska, "Optimum plane selection criteria for single-beam phase retrieval techniques based on the contrast transfer function," Opt. Lett. **39**(1), 30–33 (2014).
9. J. Martinez-Carranza, K. Falaggis, and T. Kozacki, "Optimum measurement criteria for the axial derivative intensity used in transport of intensity-equation-based solvers," Opt. Lett. **39**(2), 182–185 (2014).
10. K. Falaggis, T. Kozacki, and M. Kujawinska, "Accelerated single-beam wavefront reconstruction techniques based on relaxation and multiresolution strategies," Opt. Lett. **38**(10), 1660–1662 (2013).
11. C. J. R. Sheppard, "Defocused transfer function for a partially coherent microscope and application to phase retrieval," J. Opt. Soc. Am. A **21**(5), 828–831 (2004).
12. C. Falldorf, C. von Kopylow, and R. B. Bergmann, "Wave field sensing by means of computational shear interferometry," J. Opt. Soc. Am. A **30**(10), 1905–1912 (2013).
13. D. Gabor, "A new microscopic principle," Nature **161**(4098), 777–778 (1948).
14. M. Guizar-Sicairos and J. R. Fienup, "Understanding the twin-image problem in phase retrieval," J. Opt. Soc. Am. A **29**(11), 2367–2375 (2012).
15. K. Creath, "Phase-measurement interferometry techniques," in Progress in Optics, E.Wolf, ed. (Pergamon, NewYork, 1988), **26**, 350–393.

#224438 - $15.00 USD Received 6 Oct 2014; revised 2 Dec 2014; accepted 6 Dec 2014; published 4 Feb 2015

16. J. Glückstad and P. C. Mogensen, "Optimal phase contrast in common-path interferometry," Appl. Opt. **40**(2), 268–282 (2001).
17. G. Popescu, L. P. Deflores, J. C. Vaughan, K. Badizadegan, H. Iwai, R. R. Dasari, and M. S. Feld, "Fourier phase microscopy for investigation of biological structures and dynamics," Opt. Lett. **29**(21), 2503–2505 (2004).
18. R. Porras Aguilar, J. C. Ramirez-San-Juan, O. Baldovino-Pantaleon, D. May-Arrioja, M. L. Arroyo Carrasco, M. D. Iturbe-Castillo, D. Sánchez-de-la-Llave, and R. Ramos-Garcia, "Polarization-controlled contrasted images using dye-doped nematic liquid crystals," Opt. Express **17**(5), 3417–3423 (2009).
19. C. G. Treviño-Palacios, M. D. Iturbe-Castillo, D. Sánchez-de-la-Llave, R. Ramos-García, and L. I. Olivos-Pérez, "Nonlinear common-path interferometer: an image processor," Appl. Opt. **42**(25), 5091–5095 (2003).
20. Z. Wang and B. Han, "Advanced iterative algorithm for phase extraction of randomly phase-shifted interferograms," Opt. Lett. **29**(14), 1671–1673 (2004).
21. Q. Kemao, H. Wang, W. Gao, L. Feng, and S. Hock Soon, "Phase extraction from arbitrary phase-shifted fringe patterns with noise suppression," Opt. Lasers Eng. **48**(6), 684–689 (2010).
22. J. Glückstad and D. Palima, *Generalized Phase Contrast*, Springer Series in Optical Sciences (Springer Netherlands, 2009), Vol. 146, pp. 7–12.
23. D. Sánchez-de-la-Llave and M. D. I. Castillo, "Influence of illuminating beyond the object support on Zernike-type phase contrast filtering," Appl. Opt. **41**(14), 2607–2612 (2002).
24. C. S. Anderson, "Fringe visibility, irradiance, and accuracy in common path interferometers for visualization of phase disturbances," Appl. Opt. **34**(32), 7474–7485 (1995).
25. G. A. Ayubi, C. D. Perciante, J. L. Flores, J. M. Di Martino, and J. A. Ferrari, "Generation of phase-shifting algorithms with N arbitrarily spaced phase-steps," Appl. Opt. **53**(30), 7168–7176 (2014).
26. I. Jánossy and L. Szabados, "Optical reorientation of nematic liquid crystals in the presence of photoisomerization," Phys. Rev. E Stat. Phys. Plasmas Fluids Relat. Interdiscip. Topics **58**(4), 4598–4604 (1998).
27. A. A. Rodríguez-Rosales, R. Ortega-Martínez, M. L. Arroyo Carrasco, E. Reynoso Lara, C. G. Treviño Palacios, O. Baldovino-Pantaleón, R. Ramos García, and M. D. Iturbe-Castillo, "Neither Kerr Nor Thermal Nonlinear Response of Dye Doped Liquid Crystal Characterized by the Z-Scan Technique," Mol. Cryst. Liq. Cryst. (Phila. Pa.) **489**(1), 9 (2008).
28. I.-C. Khoo, *Liquid Crystals* (John Wiley & Sons, Inc., 2007).
29. L. Marrucci and D. Paparo, "Photoinduced molecular reorientation of absorbing liquid crystals," Phys. Rev. E Stat. Phys. Plasmas Fluids Relat. Interdiscip. Topics **56**(2), 1765–1772 (1997).
30. C. R. Mercer and K. Creath, "Liquid-crystal point-diffraction interferometer for wave-front measurements," Appl. Opt. **35**(10), 1633–1642 (1996).
31. C. L. Koliopoulos, O. Kwon, R. Shagam, J. C. Wyant, and C. R. Hayslett, "Infrared point diffraction interferometer," Opt. Lett. **3**(3), 118–120 (1978).
32. T. Hoang, Z. Wang, M. Vo, J. Ma, L. Luu, and B. Pan, "Phase extraction from optical interferograms in presence of intensity nonlinearity and arbitrary phase shifts," Appl. Phys. Lett. **99**(3), 031104 (2011).
33. T. Kozacki, K. Falaggis, and M. Kujawinska, "Computation of diffracted fields for the case of high numerical aperture using the angular spectrum method," Appl. Opt. **51**(29), 7080–7088 (2012).

1. Introduction

The visualization of phase objects [1,2] had a tremendous impact in science and technology, because it allowed revealing hidden features of the objects under investigation. The popularity and usefulness of these techniques were accompanied by phase measuring techniques [3] in form of shearing [4], interferometry [5], or holography [6] techniques, or by techniques that obtain the phase estimate from defocus [7–11]. Recent advances in shearing techniques [12] give a robust measurement configuration with high accuracy that allows a direct phase reconstruction. The drawback of these techniques lies in the system complexity that demands a specific form of illumination as well as an additional computational effort during the phase reconstruction procedure. Conventional inline-holographic techniques [13] offer a phase measuring capability in simple measurement setups. However, the phase reconstruction is limited by the presence of the twin-image and further computations are needed within twin-removal techniques [14]. Interferometry and holography based measurement systems employing temporal phase shifting techniques [15] do not require such effort and give an instant result. However, these devices are sensitive to environmental vibrations. Single shot spatial carrier techniques allow the reconstruction from a single frame, but require a fringe pattern analysis and give usually a lower resolution and accuracy [3]. Common path (CP) configurations [16] as point diffraction interferometers (PDI) do not have such drawbacks. Quantitative phase measurements have been reported in a CP system using spatial light modulators (SLMs) in order to induce controllable phase shifts to the zero-

#224438 - $15.00 USD Received 6 Oct 2014; revised 2 Dec 2014; accepted 6 Dec 2014; published 4 Feb 2015

frequency of the intensity distribution at Fourier plane [17]. An SLM may modulate the zero-frequency using a single or a few pixels, however, the dimensions of the pixels only allow obtaining an optimal CP configuration for specific optical systems. The use of optical nonlinear materials as phase shifting devices in common path configurations has been reported by numerous authors [18,19]. These systems are self-aligned and have a tunable self-induced phase shift at the Fourier plane, due to the nonlinear optical behavior of the material. However, the complexity of those systems lies in the phase shift calibration due to the material nonlinearity. A similar problem is also encountered in interferometry due to the use of non-ideal phase shifters as well as a background drifts. The use of iterative random phase shifting algorithms (RPSA) [20] that extract the phase from a series of interferograms with unknown phase steps overcome this obstacle. Other random phase retrieval techniques achieve a higher accuracy, but require carrier fringes for the reconstruction [21]. Nevertheless, available RPSA have been originally developed for two-beam interferometers only and are not applicable to CP configurations, because the interferograms underlie a different image formation mechanism and have no carrier fringes.

In this work, a RPSA is reported that enables the accurate phase reconstructions in CP devices using a series of interferograms having unknown phase shifts. This RPSA is derived from a complete framework that describes the image formation in CP configurations using a so-called Generalized Phase Contrast (GPC) theory [22]. The GPC theory includes a non-uniform background modulation and varying visibility due to the influence of various parameters including size of the phase filter at the Fourier plane, as well as fill factor [23]. Hence, the GPC [22] based RPSA presented here uses an image formation model that gives an accurate description between the phase of the object $\varphi(x,y)$, phase step θ_n of the phase filter and intensity $I_n(x,y)$. This technique is referred to as common path random phase shifting algorithm (CP-RPSA). The paper is organized as follows: Section 2 derives the theory of temporal phase shifting techniques in common-path interferometry for both, the case of known (Section 2.1) and unknown (Section 2.2) phase shifted interferograms. The validity of these techniques is verified experimentally in Section 3, where further discussion follow in Section 4. The conclusions are presented in Section 5.

2. Quantitative phase imaging in common-path systems

2.1 Temporal phase shifting techniques

Consider a CP configuration with a step-like filter placed at the Fourier plane as shown in Fig. 1. The intensity distribution $I_n = I_n(x,y)$, at the output plane with spatial coordinates x and y, has an interdependence with the phase object $\varphi = \varphi(x,y)$, and the phase shift θ_n as [16],

$$I_n \cong (A\beta_0)^2 \left|\exp(i\varphi) + C\,[\beta_0^{-1}\beta_1 \exp(i\theta_n) - 1]\right|^2, \qquad (1)$$

where A is the amplitude of the optical field, β_0 is the transmittance for spatial frequency components exceeding the radius of the circular filter R_1 (Fig. 1), and β_1 and θ_n is the transmittance and the phase shift of the filter at the Fourier plane, respectively. The parameter C is a constant that can be expressed as a product of two components: $C = K\cdot|\alpha|$, where the factor K is a constant defined by experimental conditions for the system in Fig. 1 that can be calculated [16,22] as $K = 1 - J_0(1.22\pi\eta)$, where J_0 is the Bessel function of the first kind and the parameter $\eta = R_1 / R_2$, where R_2 is the radius of the main lobe of the Airy function at the Fourier plane [16]. A commonly present, but often neglected aspect in CP systems are the fill-factor requirements [23] that affect the constant $|\alpha|$ with $|\alpha|<1$. The parameter$|\alpha|$ describes the effect of the object wave that is modulated by the phase filter; however, if the object dimensions are small compared to the illumination, i.e. the fill-factor requirements are fulfilled $|\alpha|\sim 1$. An appropriate choice of K allows optimizing the measurement conditions giving highest visibility and performance [24]. A detailed analysis on K and η as well as

#224438 - $15.00 USD Received 6 Oct 2014; revised 2 Dec 2014; accepted 6 Dec 2014; published 4 Feb 2015

further expressions for K and α are derived in [16] and show that both K and η remain constant for a given measurement configuration.

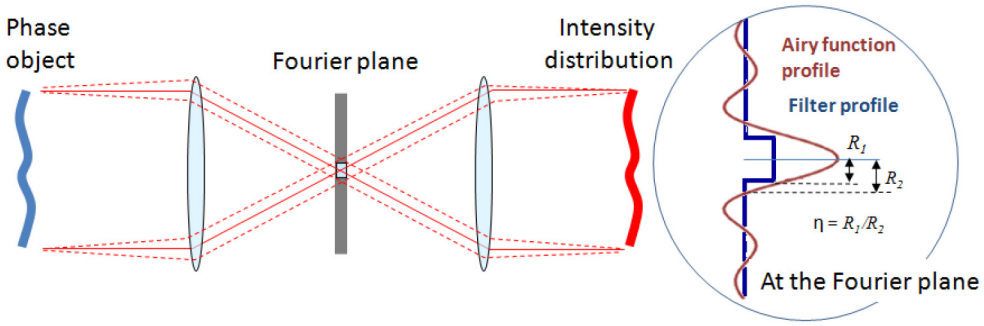

Fig. 1. Schematic of a CP-configuration having a circular phase filter at the Fourier plane.

Given these considerations, it is possible to re-express Eq. (1) after some algebraic manipulations, using the parameters $q_1 = 1 + C^2 + \beta^2 C^2$, $q_2 = -2\beta C^2$, $q_3 = 2\beta C$, and $\beta = \beta_1/\beta_0$, as

$$I_{m,n} \cong (A\beta_0)^2[q_1 + q_2\cos\varphi_m - q_3\cos\theta_n + q_3(\cos\theta_n\cos\varphi_m + \sin\theta_n\sin\varphi_m)], \quad (2)$$

where m is an integer denoting pixel numeration at the camera so that each m corresponds to a given position $m \rightarrow (x,y)$, with $m = 0, 1, \ldots, (M-1)$, and M is the total number of pixels at each frame. Notably, $\beta = 1$ for phase filters with pure phase modulation. Given these considerations, it is possible to estimate the unknown object phase from a series of N intensity measurements taken at various phase shifts θ_n. For the case of arbitrary (but known) phase steps, the phase can be estimated by solving following linear system with

$$\vec{I}_m = Q\, q\, \vec{p}_{CPm}, \quad (3)$$

with

$$Q = \begin{bmatrix} 1 & \cos\theta_0 & \sin\theta_0 \\ 1 & \cos\theta_1 & \sin\theta_1 \\ \vdots & \vdots & \vdots \\ 1 & \cos\theta_{(N-1)} & \sin\theta_{(N-1)} \end{bmatrix}, \quad (4)$$

$$q = \begin{bmatrix} q_1 & -q_3 & 0 \\ q_2 & q_3 & 0 \\ 0 & 0 & q_3 \end{bmatrix}, \quad (5)$$

$\vec{p}_{CPm} = [A^2\beta_0^2 \quad A^2\beta_0^2\cos\varphi_m \quad A^2\beta_0^2\sin\varphi_m]^T$, $\vec{I}_m = [I_{m,0} \quad I_{m,1} \quad \cdots \quad I_{m,(N-1)}]^T$, and $tan(\varphi_m) = p_{CPm(3)}/p_{CPm(2)}$, where $p_{CPm(3)}$ and $p_{CPm(2)}$ are the third and second element of the vector p_{CPm}. For comparison, for the case of an ordinary two-beam interferometer the relation between the interferometer phase and the intensity is given as

$$\vec{I}_m = Q\,[A^2 \quad A^2\gamma\cos\varphi_m \quad A^2\gamma\sin\varphi_m]^T, \quad (6)$$

where γ is the fringe visibility. Usually, the accuracy in the phase estimate when using Eq. (3) is limited by the presence of intensity noise and phase shift errors.

#224438 - $15.00 USD Received 6 Oct 2014; revised 2 Dec 2014; accepted 6 Dec 2014; published 4 Feb 2015

If a dye doped LC material is used as a phase filter, there are time-variant phase shift errors due to the presence of intensity noise, polarization stability, temperature changes, and molecular misalignments. Hence, modelling of the phase shift error using time-invariant models as it is the commonly adopted in interferometry [25] would not be appropriate, when e.g. characterizing the nonlinear response of piezo electric transducer based phase shifting units with a linear and quadratic term.

2.2 Phase reconstructions from random phase shifted interferograms

In the following a GPC based random phase shifting algorithm is derived that accounts for these errors. Consider an alternative calculation of the vector p_{CPm} in Eq. (3) using a least-square criterion [20] as

$$S_f = \sum_{n=0}^{N-1} (f_{(1)} + \cos\theta_n \; f_{(2)} + \sin\theta_n \; f_{(3)} - I_{m,n})^2, \tag{7}$$

with $\vec{f} = q \; \vec{p}_{CPm}$, where for the correct phase step θ_n one obtains $\partial S_f / \partial f_{(1)} = 0, \partial S_f / \partial f_{(2)} = 0, \partial S_f / \partial f_{(3)} = 0$, and

$$A q \; \vec{p}_{CPm} = [\sum_{n=0}^{N-1} I_{m,n} \quad \sum_{n=0}^{N-1} I_{m,n} \cos\theta_n \quad \sum_{n=0}^{N-1} I_{m,n} \sin\theta_n]^T, \tag{8}$$

where

$$A = \begin{pmatrix} N & \sum_{n=0}^{N-1} \cos\theta_n & \sum_{n=0}^{N-1} \sin\theta_n \\ \sum_{n=0}^{N-1} \cos\theta_n & \sum_{n=0}^{N-1} \cos^2\theta_n & \sum_{n=0}^{N-1} \sin\theta_n \cos\theta_n \\ \sum_{n=0}^{N-1} \sin\theta_n & \sum_{n=0}^{N-1} \sin\theta_n \cos\theta_n & \sum_{n=0}^{N-1} \sin^2\theta_n \end{pmatrix}. \tag{9}$$

Similar to the case of Eq. (3), the phase φ_m at every pixel can be calculated as $tan(\varphi_m) = p_{CPm(3)} / p_{CPm(2)}$ using

$$\vec{p}_{CPm} = [A q]^{-1} [\sum_{n=0}^{N-1} I_{m,n} \quad \sum_{n=0}^{N-1} I_{m,n} \cos\theta_n \quad \sum_{n=0}^{N-1} I_{m,n} \sin\theta_n]^T. \tag{10}$$

Once the phase φ_m is estimated, it is possible to use this information in order to get a better estimate for the individual phase steps θ_n. The intensity $I_{m,n}$ can be expressed using the n^{th} row of the matrix Q (denoted as Q_n) as

$$I_{m,n} = Q_n \; q \; \vec{p}_{CPm}. \tag{11}$$

Being a scalar, $I_{m,n}$ can be written, using $I_{m,n} = I_{m,n}^T$, *as*

$$\begin{aligned} I_{m,n} &= \vec{p}_{CPm}^T \; q^T Q_n^T \\ &= g_{(1)} + \cos\varphi_m \; g_{(2)} + \sin\varphi_m \; g_{(3)}, \end{aligned} \tag{12}$$

where $\vec{g} = q^T \vec{h}$ and $\vec{h} = [A^2\beta_0^2 \quad A^2\beta_0^2 \cos\theta_n \quad A^2\beta_0^2 \sin\theta_n]^T$. Similar to the case of Eq. (7), when defining a least square criterion of the RPSA in [20], as

$$S_g = \sum_{m=0}^{M} (g_{(1)} + \cos\varphi_m \; g_{(2)} + \sin\varphi_m \; g_{(3)} - I_{m,n})^2 \tag{13}$$

#224438 - $15.00 USD Received 6 Oct 2014; revised 2 Dec 2014; accepted 6 Dec 2014; published 4 Feb 2015

and using $\partial S_g / \partial g_{(1)} = 0, \partial S_g / \partial g_{(2)} = 0, \partial S_g / \partial g_{(3)} = 0$, one obtains

$$B\, q^T \vec{h} = [\sum_{m=0}^{M-1} I_{m,n} \quad \sum_{m=0}^{M-1} I_{m,n} \cos\varphi_m \quad \sum_{m=0}^{M-1} I_{m,n} \sin\varphi_m]^T, \tag{14}$$

where M is the total number of pixels, and

$$B = \begin{pmatrix} M & \sum_{m=0}^{M-1} \cos\varphi_m & \sum_{m=0}^{M-1} \sin\varphi_m \\ \sum_{m=0}^{M-1} \cos\varphi_m & \sum_{m=0}^{M-1} \cos^2\varphi_m & \sum_{m=0}^{M-1} \sin\varphi_m \cos\varphi_m \\ \sum_{m=0}^{M-1} \sin\varphi_m & \sum_{m=0}^{M-1} \sin\varphi_m \cos\varphi_m & \sum_{m=0}^{M-1} \sin^2\varphi_m \end{pmatrix}. \tag{15}$$

The phase step at each phase shift angle θ_n is then calculated as $tan(\theta_n) = h_{(3)} / h_{(2)}$ using

$$\vec{h} = [Bq^T]^{-1} [\sum_{m=0}^{M-1} I_{m,n} \quad \sum_{m=0}^{M-1} I_{m,n} \cos\varphi_m \quad \sum_{m=0}^{M-1} I_{m,n} \sin\varphi_m]^T. \tag{16}$$

Similar to the case of interferometry [20], it is possible to apply an iterative procedure to estimate both φ_m and θ_n. This eight steps procedure is referred to as a common path random phase shifting algorithm (CP-RPSA) and is carried out as follows:

1) The phase steps θ_n are initialized using a randomly chosen value or a rough pre-estimate that may be obtained from measurements of known objects using the same measurement device.

2) The matrix A of Eq. (9) is computed using all (θ_n) *'s.*

3) The vector p_{CPm} is calculated using Eq. (10) for *each* pixel m.

4) The φ_m is calculated at *each* pixel using $tan(\varphi_m) = p_{CPm(3)} / p_{CPm(2)}$.

5) The matrix B of Eq. (15) is computed using all (φ_m) *'s.*

6) The vector h is calculated using Eq. (16) for *each* intensity frame captured at the phase step θ_n.

7) The phase step θ_n is calculated for *each* frame using $tan(\theta_n) = h_{(3)} / h_{(2)}$.

8) The steps 2 to 7 are repeated until the values of θ_n converge, i.e. the maximum difference in all θ_n between two subsequent iterations falls below a certain threshold e.g. $| \theta_n - \theta_{n+1} | < 10^{-10}$.

It should be noted that this train of thought is equal to the RPSA of [20] for the case of a two-beam interferometer, i.e. Equation (6) instead of Eq. (3) is adopted for the derivation; this assumption however cannot be made in common-path configurations.

2.3 Simulations

The CP-RPSA approach presented here as well as the necessity of the GPC model have been verified by simulation. An example of the discrepancy in the reconstructed phase when assuming a two-beam interferometry model (i.e. solution to Eq. (6)) and a GPC based image formation (i.e. solution to Eq. (3)) is shown in Fig. 2. The simulations in Fig. 2 have been carried out for a pure phase object in form of a Lena phantom with a maximum phase difference of 1.7π that is measured in a CP configuration with $C = 0.9$, $N = 4$, and $\theta_n = (n-1)\, \pi/2$, i.e. the image formation follows Eq. (1). The first problem that is encountered when assuming a two-beam interferometer based image formation, is that the conventional RPSA

#224438 - $15.00 USD Received 6 Oct 2014; revised 2 Dec 2014; accepted 6 Dec 2014; published 4 Feb 2015

of reference [20] does not converge, even under ideal conditions i.e. in absence of noise and no phase shift miscalibrations. Certainly, for the latter case with the particular interferometry based image formation model it is possible to obtain a solution by solving Eq. (6) directly by assuming that the phase steps are known. The results are shown in Fig. 2a.

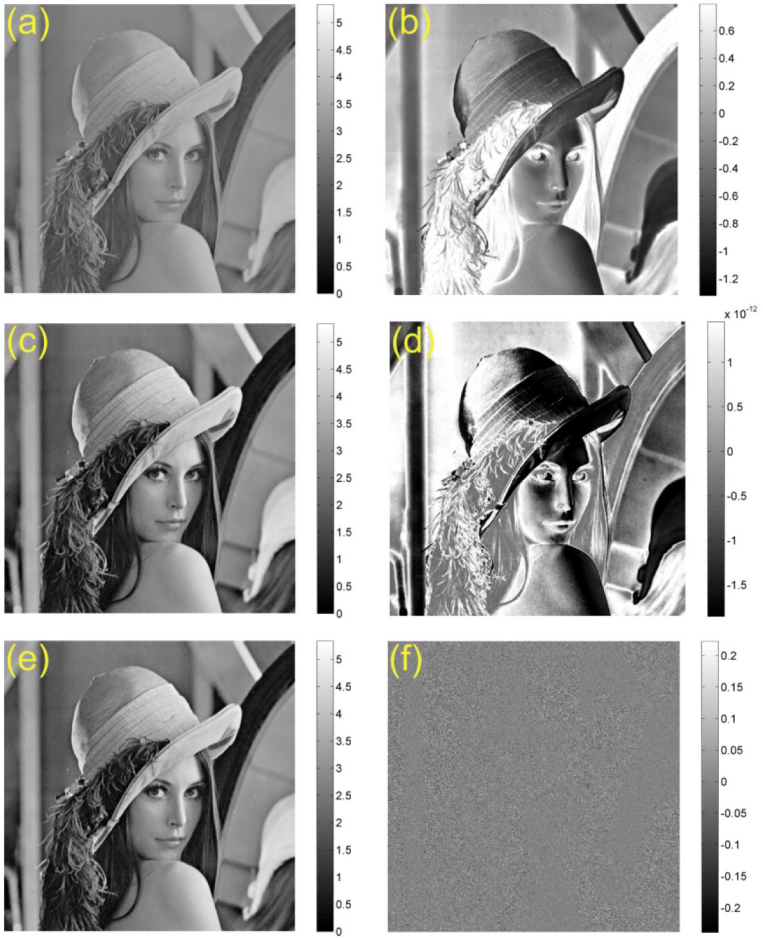

Fig. 2. Phase reconstructions in a common path configuration described by Eq. (1) for a Lena phantom with a maximum phase difference of 1.7π for the case of $N = 4$, and $\theta_n = (n-1)\,\pi/2$, with $n = 0, 1, 2, 3$ when using (a) interferometry based reconstruction (direct solution to Eq. (6)) and (c) the CP-RPSA presented here. The corresponding error for (a) and (c) is shown in (b) and (d), respectively. The case of (c,d) is shown in (e,f) but having AWGN with $\sigma_I = 0.05$. All units are in radians.

The error for the noise free case indicates (see Fig. 2b) the presence of systematic errors that can be traced back to the assumption of two-beam interferometry (validity of Eq. (6)). On the contrary, when using the CP-RPSA procedure presented here, an exact reconstruction is achieved at the accuracy limit of double precision computations. The recovered phase and phase error is shown in Fig. 2c and 2d, respectively. The robustness of this method is verified for the case of additive white Gaussian noise (AWGN) with a (to one) standard deviation in the measured intensity σ_I of $\sigma_I = 0.05$ as shown in Figs. 2e and 2f. The results indicate that a robust phase reconstruction can be achieved when using this GPC based methodology.

A further analysis on the noise dependency of the CP-RPSA algorithm is shown in Table 1 for $N = 4$ (cases 1 to 4) and $N = 5$ (cases 5 to 8) in presence of various levels of noise.

#224438 - $15.00 USD Received 6 Oct 2014; revised 2 Dec 2014; accepted 6 Dec 2014; published 4 Feb 2015

Table 1 represents a typical experimental situation where one seeks to obtain a series of phase shifted interferograms with a phase step of $2\pi/N$, but due uncertainties the actual phase shift has an error. In the simulations for Table 1, the real phase shifts for $N = 4$ equals $\theta_1 = -0.267$, $\theta_2 = 1.628$, $\theta_3 = 2.819$, and $\theta_4 = -1.164$, and for the case of $N = 5$ there are $\theta_1 = -0.534$, $\theta_2 = 1.372$, $\theta_3 = 1.868$, $\theta_4 = -1.700$, and $\theta_5 = 0.856$. The results in Table 1 indicate, that in presence of no noise, the CP-RPSA recovers the real phase shift very well giving a negligible error in the reconstructed phase. In presence of noise however, there is a mismatch between the real and the recovered phase step, which results in non-ideal phase reconstructions. The root mean square error (RMSE) for the phase of these cases is shown in Table 1, which indicate an acceptable level of accuracy. For comparison, when solving Eq. (3) directly (assuming a constant phase step of $2\pi/N$) the RMSE in the recovered phase is equal to 0.0351 (case 1), 0.0355 (case 2), 0.0367 (case 3), 0.0387 (case 4), 0.0812 (case 5), 0.0815 (case 6), 0.0820 (case 7), and 0.0832 (case 8) radians. The results indicate that a significantly higher accuracy is achievable when using the CP-RPSA algorithm instead of solving Eq. (3) directly.

Table 1. Comparison of the real and recovered phase shift as well as RMSE of the recovered phase when using CP-RPSA algorithm with $N = 4$ (cases 1-4) and $N = 5$ (cases 5-8) for various levels of noise (σ_I). All units are in radians.

Simulation cases	Real phase step					Estimated phase step CP-RPSA					RMSE
	θ_1	θ_2	θ_3	θ_4	θ_5	θ_1	θ_2	θ_3	θ_4	θ_5	phase
1 $\sigma_I = 0$	-0.267	1.628	2.819	-1.164	-	-0.267	1.628	2.819	-1.164	-	2e-12
2 $\sigma_I = 0.01$	-0.267	1.628	2.819	-1.164	-	-0.258	1.610	2.819	-1.155	-	0.0055
3 $\sigma_I = 0.02$	-0.267	1.628	2.819	-1.164	-	-0.237	1.575	2.824	-1.117	-	0.0116
4 $\sigma_I = 0.03$	-0.267	1.628	2.819	-1.164	-	-0.206	1.520	2.844	-1.043	-	0.0198
5 $\sigma_I = 0$	-0.534	1.372	1.868	-1.700	-0.856	-0.534	1.372	1.868	-1.700	-0.856	1e-12
6 $\sigma_I = 0.01$	-0.534	1.372	1.868	-1.700	-0.856	-0.530	1.369	1.863	-1.697	-0.854	0.0041
7 $\sigma_I = 0.02$	-0.534	1.372	1.868	-1.700	-0.856	-0.513	1.331	1.827	-1.693	-0.829	0.0091
8 $\sigma_I = 0.03$	-0.534	1.372	1.868	-1.700	-0.856	-0.495	1.289	1.796	-1.681	-0.817	0.0142

The simulations results of Table 1 indicate that the CP-RPSA procedure has the potential to estimate the unknown phase shifts iteratively, or alternatively, in case of a fairly well known phase shift it is possible to correct for errors in the phase shift. This property is investigated for a number of cases by simulation using 100 randomly generated phase shift errors. As a measure of the discrepancy between the real phase steps $\theta_{n,real}$ and the ideal phase steps $\theta_{n,ideal}$ the so called phase shift error (PSE) is defined as,

$$PSE = \sqrt{\sum_{n=1}^{N} (\theta_{n,real} - \theta_{n,ideal})^2}. \quad (17)$$

The simulations in Fig. 3 have been carried out under the same conditions as in Fig. 2, but having various amounts of PSEs. In these simulations the CP-RPSA iterations are terminated if the RMS between two subsequent phase shifts is $< 10^{-10}$, or if a total number of 10000 iterations is exceeded. Figure 3a shows the PSE of the estimated phase shift of the CP-RPSA for a given initial PSE of the measurement system. The results indicate that PSEs can be significantly reduced when using the CP-RPSA algorithm.

The corresponding RMSE of the object phase is shown in Fig. 3b (blue): similar to the case of Fig. 3a, for most cases a significantly reduced error in the reconstructed object phase is obtained, giving higher accuracy. For comparison, the RMSE in Fig. 3b is shown as well for the case when solving Eq. (3) directly (red). It should be noted however, that in some cases the CP-RPSA did not converge and the phase shift error could not be corrected. Those cases occur if the CP-RPSA is trapped in a local minimum and typically show an oscillatory behaviour in the difference between two subsequent estimates of the phase shift. This difference may be small, but becomes larger with increasing number of iterations, before it gets smaller again, and continuously cycles in this manner. Nevertheless, such cases can be detected, as the difference between two subsequent phase shifts is typically larger than the

#224438 - $15.00 USD Received 6 Oct 2014; revised 2 Dec 2014; accepted 6 Dec 2014; published 4 Feb 2015

threshold, i.e. $|\theta_n - \theta_{n+1}| > 0.1$ radians, even after a very large number of iterations (e.g. 10000). In those cases it is advisable to restart the CP-RPSA with different initial conditions (e.g. using randomly chosen phase shifts) or to repeat the measurement; commonly these measures are sufficient.

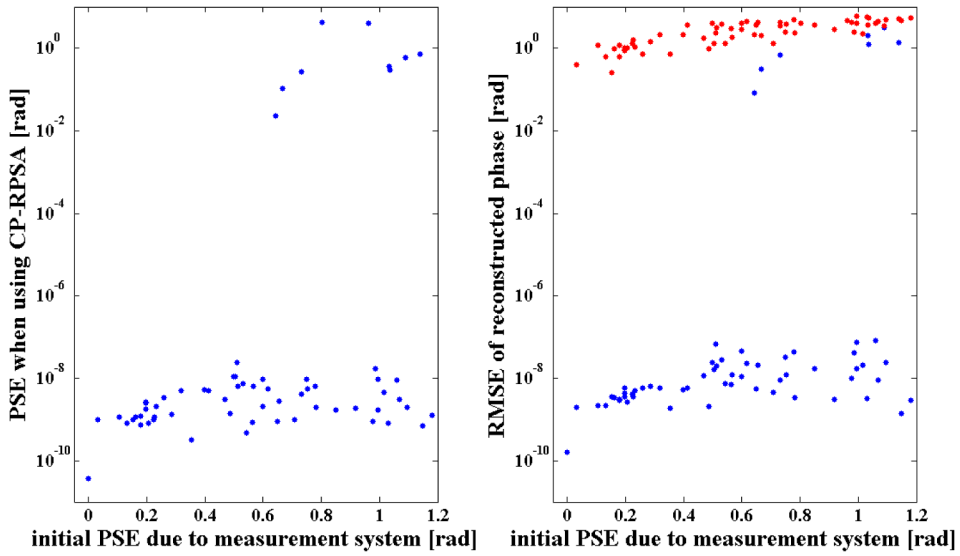

Fig. 3. Phase reconstructions for the case of Fig. 2, but having various phase shift errors. Figure 3a shows the PSE that is obtained by the CP-RPSA for a given PSE of the measurement system. Figure 3b shows the RMSE of the reconstructed phase when using the CP-RPSA algorithm (blue) or when solving Eq. (3) directly (red). All units are in radians. Each dot corresponds to one out of 100 simulations.

3. Experiments

The setup of the CP system used for the measurements in this work is depicted in Fig. 4. The dye doped LC cell (reported in [18]) is placed at the Fourier plane. The half-wave plate allows altering the polarization and thereby controls the phase shift of the active filter [18]. In this way, a series of interferograms can be recorded having various phase shifts.

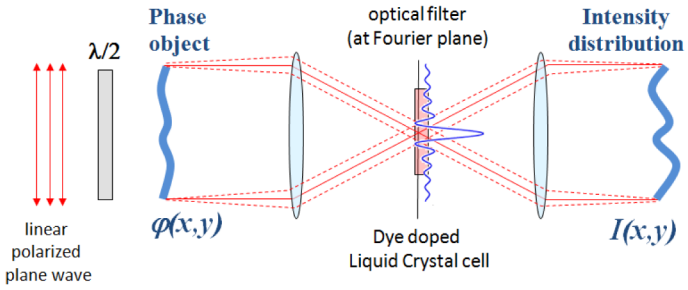

Fig. 4. Schematic of the nonlinear phase contrast microscope with a polarization controlled phase shift.

The measurement in Fig. 5 shows three different rectangular shaped step-like phase objects with a maximum step of ~600nm (a,d), ~320nm (b,e), and ~150nm (c,f) that is illuminated with λ = 633nm. The measurements in Fig. 5 have been conducted in the setup of Fig. 4 with $K \sim 0.761$ and $\eta \sim 0.515$ using a series of 19 intensities obtained with various phase shifts. Similar to the case of Fig. 2, the use of the conventional RPSA [20] was not successful, because no convergence could be observed for any of the recorded data sets. Solutions to Eq.

#224438 - $15.00 USD Received 6 Oct 2014; revised 2 Dec 2014; accepted 6 Dec 2014; published 4 Feb 2015

(6) (two-beam Interferometry) can therefore only be carried out when assuming the case of no phase shift errors in the assumed phase shift. The phases in (a,b,c) correspond to this particular case and have been reconstructed by solving Eq. (6) directly for a set of phase shifts (assumed to be known). Nevertheless, despite the common believe even for very well calibrated systems with known phase steps, the assumption of a two-beam interferometer is wrong: the reconstructed objects in (a,b,c) have for all three cases a much larger phase difference than the expected known phase distribution of the manufactured object. On the contrary, when using the CP-RPSA procedure of Section 2.2 that is based on the GPC model [16,22], the recovered phases are in good agreements with the expected object phase distributions, as it is shown in Fig. 5 (d, e, f).

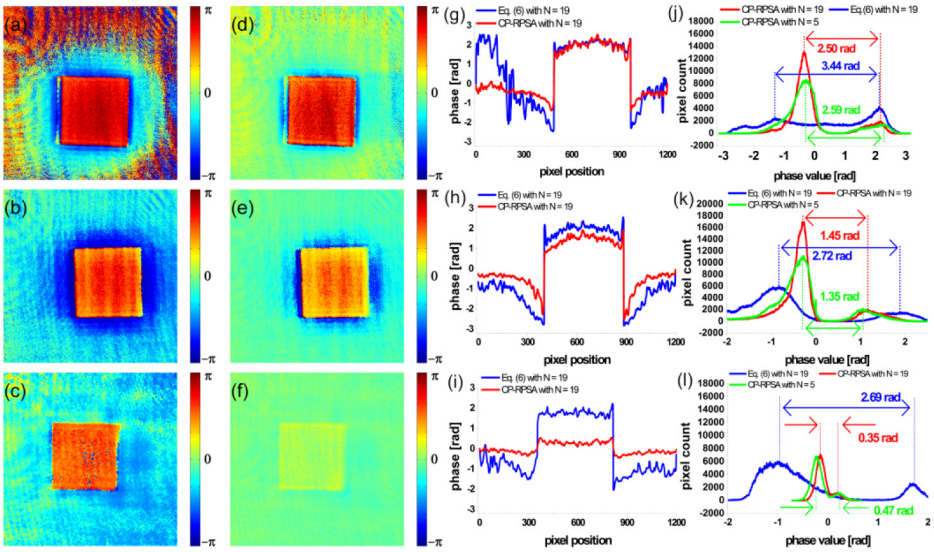

Fig. 5. Measurement of a step-like phase object with a maximum step of 2.8 radians (a,d), 1.5 radians (b,e), and 0.7 radians (c,f). The phases in (a,b,c) and (d,e,f) correspond to the direct solution of Eq. (6) and the GPC based CP-RPSA solution, respectively. A phase cut through the center of the object (g, h, i) and a histogram of the phase values (j, k, l) is shown in the equivalent figure row. A median filter of size 9x9 and an offset correction has been applied to the figures (g) to (l) for better visualization. The measurements have been conducted in the setup of Fig. 4 using a wavelength of 633nm with $K \sim 0.761$. All units are in radians.

A phase cut through the center of the object (g, h, i) and a histogram of the phase values (j, k, l) highlight these results and are shown in the equivalent figure row of Fig. 5, for the case of Eq. (6) with $N = 19$ (blue curve) and the CP-RPSA algorithm with $N = 19$ (red curve). For comparison, the histogram of a CP-RPSA based phase reconstruction with $N = 5$ is plotted as well (green curve). Figure 6 shows the estimated phase shifts θ_n for the case of Fig. 5d, which show to follow a sinusoidal curve when stepping linearly the polarization angle of the illumination wave. This trend is expected, due to the polarization based phase shifting technique in Fig. 4. The sinusoidal behavior originates from the dependence of the phase shift as function of the direction of polarization with respect to the alignment of the liquid crystal molecules and coincides with theoretical predictions [18,26,27], i.e. as reported in [18],

$$\theta_n \approx \Phi_N \cos^2 \Psi_n + \Phi_P \sin^2 \Psi_n \qquad (18)$$

where Ψ_n is the angle of the incident polarization, Φ_N and Φ_P are the on-axis phase changes for 0 and 90 degree input polarization. It should be noted, that once a measurement is carried out, the results of Fig. 6 could be used as a pre-estimate of the phase shift for future

#224438 - $15.00 USD Received 6 Oct 2014; revised 2 Dec 2014; accepted 6 Dec 2014; published 4 Feb 2015

measurements; the task of the CP-RPSA algorithm is then to remove the PSE of the non-linear phase filter response.

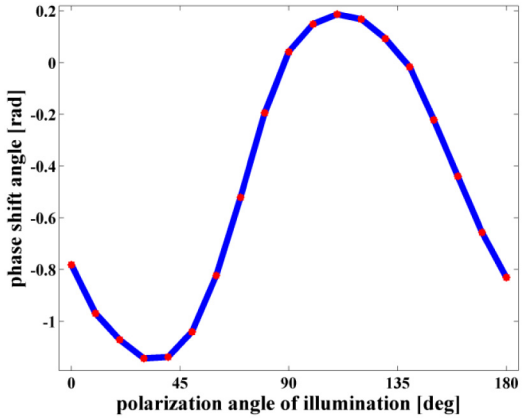

Fig. 6. Sinusoidal behaviour of the estimated phase shifts θ_n for the case of Fig. 5d

Another application of this quantitative phase imaging technique is given in the field of life-sciences, where the aim is to obtain a quantitative estimate of the morphology of a label-free biological sample. Figure 7 shows these measurement results for a single protozoan using the system depicted in Fig. 4, where a series of 3 interferograms have been obtained. Figure 7a, 7b, and 7c show the recorded intensities at the phase shift angles of –0.490, –0.117, and 0.142 radians, respectively. For visualization purposes only the first 120 out 256 gray levels are shown. The reconstructed wrapped and unwrapped phase is shown in Fig. 7d and 7e, respectively. It is interesting to notice that once a quantitative phase estimate is obtained, it is possible to simulate any view that would be obtained in different microscope configuration: Fig. 7f shows an example of an equivalent view in differential interference microscopes (DICs).

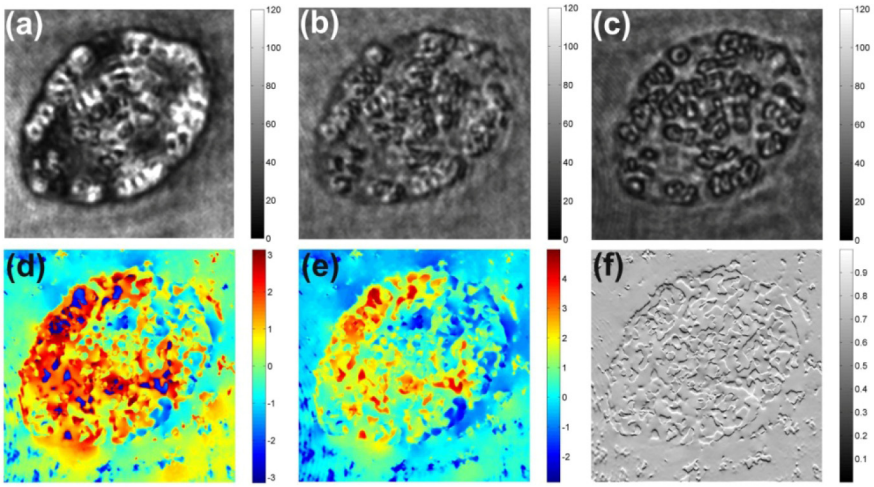

Fig. 7. Quantitative phase imaging for an unlabelled biological object (protozoan) using the measurement system of Fig. 4. Fig (a), (b), and (c) show the recorded intensities at the phase shift angles of –0.490, –0.117, and 0.142 radians, where only the first 120 gray levels are shown for better visualization. The wrapped and unwrapped phase in radians is shown in (d) and (e) respectively. The phase in (d) is used to simulate equivalent DIC view, which is shown in (f).

#224438 - $15.00 USD Received 6 Oct 2014; revised 2 Dec 2014; accepted 6 Dec 2014; published 4 Feb 2015

4. Discussions

4.1 Optimal common path configurations

The self-calibrating CP technique presented here takes advantage of the polarization controlled nonlinearity of the optical phase filter in order to obtain an optimal common path interferometer. The shape and width of the phase filter do not change with polarization, because the intensity profile of the illumination beam remains unchanged. It should be noted however, that there is a lower threshold for the induced phase shift due to the Frederick transition as well as an upper bound of the possible phase change due to saturation [28]. The threshold of the Frederick transition can be altered via voltage and the maximum phase change due to saturation depends on the cell thickness [29]. A suitable non-linear material keeps the contribution of the side-lobes below the threshold of the Frederick transition. Due to this effect, the width of the resulting phase filter is always smaller than the main lobe of the Airy function at the Fourier plane (see Fig. 1). This allows operating the CP system under optimal conditions [16] with respect to flatness of the reference beam, and visibility, i.e. giving $0.4 < \eta < 0.627$, where $\eta = R_1 / R_2$, R_1 is the radius of the phase filter, and R_2 is the radius of the main lobe of the Airy function at the Fourier plane [16]. Notably, as described by Gluckstadt [16], such values of η would not be obtained when using pixelated SLMs, because the actual value of η only optimizes specific CP configurations, where the optical system matches the pixel size or multiples of this. For comparison, static optical filters as reported by Creath [30] and Koliopoulos [31] achieve a value of $\eta \sim 3$ and $\eta \leq 0.5$, respectively, where notably the latter system operates in the infrared regime.

4.2 Minimal system calibration requirements

The quantitative phase measuring technique presented in Section 2 allows estimating the object phase from a series of phase shifted interferograms that are obtained in a CP configuration with unknown phase shifts, but takes into account the GPC based image formation that is represented by the matrix q. Notably, as it is the case for all phase shifting algorithms in CP systems, a given knowledge of the constant C is required to calculate the phase estimate, i.e. for the CP-RPSA presented here to calculate the matrix q. Usually, the constant C is estimated within the system calibration (see [17] and other literature by the same author). For an optimized system however, the constant C can be estimated in a simpler way. An example is presented in the following: consider an optimized common-path system, where the value of η is between 0.4 to 0.627, so that the values of K are found between 0.506 to 1. Because the system has to fulfil the fill-factor requirements (e.g. the illumination area is at least 10 times larger than the object area), one obtains $|\alpha| \sim 1$ and $C = K$, and therefore a value of C in the range between 0.506 to 1. For those optimized systems, it has been observed that the measurement and CP-RPSA based reconstruction of a known phase object can only be achieved for the correct choice of C, where accurate estimates give highest convergence speed. Usually, the impact of the actual value of C on the CP-RPSA convergence is very strong, small deviations of the real value of C increase significantly the number of iterations, e.g. a few 10 iterations become a few hundred iterations. Moreover, wrong values of C may even cause the solver to be trapped in a local minimum. This observation may be used to either refine the initial estimate of C, or estimate the value of C using no calibration data. In this way the actual value of C is estimated.

Furthermore, the fill-factor requirements of CP systems [23] imply that the object dimensions are small compared to the illumination, i.e. $|\alpha| \sim 1$, so that changes in the constant C with $C = K \cdot |\alpha|$ are negligible. During the calibration procedure it is possible to verify this condition using known phase objects. Once the system is adjusted and calibrated, quantitative measurements of phase objects are possible without the need of phase shift calibrations.

#224438 - $15.00 USD Received 6 Oct 2014; revised 2 Dec 2014; accepted 6 Dec 2014; published 4 Feb 2015

5. Conclusions

This work presents a self-calibrating phase shifting algorithm for quantitative phase measurements in CP configurations from interferograms with arbitrary and unknown phase shifts. Section 2.1 derives an algorithm that allows estimating the phase from a series of arbitrary but known phase shifts, which equations include the GPC based image formation. The influence of the GPC theory is represented by the matrix q, which in case of classical two-beam interferometry would not exist (compare Eq. (3) with Eq. (6)). Nevertheless, the model of classical interferometry cannot be applied to CP-configurations: it is shown that the direct solution to Eq. (6) leads to severe errors, as it is shown in Fig. 2. On the contrary, when using the GPC based CP-RPSA, an accurate result is obtained for both the case of no noise and AWGN with $\sigma_I = 0.05$ (see Fig. 2). The simulations indicate the importance of GPC based reconstructions. The simulations in Fig. 3 further verify the accuracy of this approach, and show that the CP-RPSA allows correcting for phase shift errors and thereby improving significantly the reconstruction accuracy. Notably, the principle of this algorithm is based on the RPSA algorithm of reference [20], however, more sophisticated techniques may be employed that account for harmonics in the measured intensity similar to the case of [32].

The approach presented here has also been verified experimentally using a non-linear phase contrast microscope that has a dye doped LC as an active phase filter at the Fourier plane. The phase change in the LC material is self-induced by its optical non-linearity giving a self-aligned phase filter with optimum dimensions with respect to the illumination beam. The diminutive size of these phase filters depends only on the width of the focussed incident illumination. It is shown that it is possible to operate a CP configuration with $\eta \sim 0.515$, a value that is estimated to be (according to the GPC theory [16]) in the optimal range of $0.4 < \eta < 0.627$. An appropriate choice of the nonlinear material [28] allows creating experimental conditions that provide a good compromise between a low curvature [16] and a large amplitude [24] of the reference wave for imaging systems that fulfil the fill-factor requirements [23]. It is shown that this technique can be employed in CP systems, which use highly nonlinear LC based phase filters. The major difficulty in handling those types of filters is given by the accurate phase shift calibration due to a number of time-variant error sources. This work shows how this problem is overcome when employing the self-calibrating CP-RPSA that is derived in Section 2.2. In this way, quantitative phase measurements are possible. This is verified experimentally using the measurement device of Fig. 4 [18] and a series of well-known phase objects (see Fig. 5). Furthermore, as shown in Fig. 7, the measurement techniques presented here can also be applied to the field of a label-free quantitative phase imaging of biological samples using only three images. Once the phase of the object is obtained, it is possible to refocus the field to a different plane using e.g. the angular spectrum method [33], or to digitally create views that would be obtained in various microscopes. Figure 6f shows the example of an equivalent DIC view that is obtained digitally from the quantitative phase measurement.

On a final note, LC phase filters used in those CP configurations have unique advantages in terms of cost-effectiveness and performance for a wide range of optical systems (due to the low value of η, see Section 4 and reference [16]) when compared to SLM based solutions that have a fixed pixel size and thereby only operate optimal for a specific optical configuration. For the particular system in Fig. 4, one can achieve measurements at higher temporal bandwidths by replacing the half-wave plate with a voltage controlled LC based polarization rotator.

The quantitative phase measurement technique reported here has numerous applications in the wavefront sensing, optical metrology, microscopy, and label-free quantitative phase imaging of biological samples.

#224438 - $15.00 USD Received 6 Oct 2014; revised 2 Dec 2014; accepted 6 Dec 2014; published 4 Feb 2015

Acknowledgments

R. Porras-Aguilar acknowledges the support of the Mexican Science Council, CONACyT through the Catedra-2066, K. Falaggis acknowledges the support of the statutory funds of Warsaw University of Technology, R. Ramos-Garcia acknowledges support from CONACyT under grant 153463.

#224438 - $15.00 USD Received 6 Oct 2014; revised 2 Dec 2014; accepted 6 Dec 2014; published 4 Feb 2015